# Numerical Weather Prediction

## Crisis Area Model Precipitation Imagery Over All Terrain

**Forecasting Research Technical Report No. 467**

**Una O'Keeffe**

*email: nwp_publications@metoffice.gov.uk*

# ABSTRACT

Precipitation imagery over the ocean for Europe and the North Atlantic has been produced routinely from locally received passive microwave satellite data. Difficulty in interpretation of these measurements over surfaces other than open water has previously restricted the imagery product to the ocean. However, recent advances have demonstrated that an all-terrain product is now possible, with a horizontal resolution of about 17km, allowing such images to become useful in such areas as the Middle East. To provide this in a timely fashion data from the EUMETSAT ATOVS Retransmission Service (EARS) is exploited.

The imagery, which shows the location and relative intensity of precipitation, is useful in its own right for nowcasting, and can also be used in assessment of short range forecasts, giving confidence or otherwise in the subsequent development of rain cells by the model.

This report describes the calculation of an AMSU-B derived scattering index which can represent a probability of precipitation. An interpretation of the imagery is given, and a qualitative and quantitative evaluation of the imagery is described.

## Version History:

| Date | Version | Action/comments | Approval |
|---|---|---|---|
| 13/05/05 | 0.1 | Draft for consideration by S.J.English Hd(SRAG) | Approved |
| 19/05/05 | 0.2 | Draft for consideration by J.R.Eyre Hd(SA) | Modifications required |
| 31/08/05 | 0.3 | Draft revised following comments from John Eyre Hd (SA) | Approved for issue as Technical Report by John Eyre |
| 14/11/05 | 1.0 | Issued as Technical Report No. 467 | |

# Crisis Area Model Precipitation Imagery Over All Terrain

# 1. Introduction

Precipitation imagery over the ocean for Europe and the North Atlantic has been produced routinely from locally received passive microwave satellite data. Difficulty in interpretation of these measurements over surfaces other than open water has previously restricted the imagery product to the ocean. However, recent advances have demonstrated that an all-terrain product is now possible, with a horizontal resolution of about 17km, allowing such images to become useful in such areas as the Middle East. To provide this in a timely fashion data from the EUMETSAT ATOVS Retransmission Service (EARS) is exploited.

The imagery, which shows the location and relative intensity of precipitation, is useful in its own right for nowcasting, and can also be used in assessment of short range forecasts, giving confidence or otherwise in the subsequent development of rain cells by the model.

# 2. Microwave Remote Sensing of Precipitation

In the visible and infrared parts of the spectrum, clouds are opaque, and any estimation of precipitation must be inferred using cloud top measurements. At microwave frequencies, however, the radiation can penetrate the clouds as the interaction with cloud droplets is weak, providing direct information on precipitation and cloud depth.

Below about 50 GHz, the microwave frequencies lie within an atmospheric window region and are primarily sensitive to emission by water vapour, clouds, precipitation, and surface features. These channels are useful for the discrimination of surface type, liquid water in clouds, and moderate to heavy precipitation composed of liquid water.

Differences in the emissivity of surfaces are greatest at the lower frequencies (such as AMSU 23.8 and 31 GHz). The ocean has a very low and uniform emissivity (0.4 - 0.5), making oceanic areas ideal for the retrieval of cloud and precipitation properties. Over land, where surface emissivities are high and variable, the signal of atmospheric emitters (water vapour, cloud liquid water and liquid precipitation) has little effect on the satellite-observed brightness temperatures, and so the scattering signal of precipitation-sized ice particles is required for the identification of precipitation.

At higher frequencies (>50GHz) scattering from large ice particles becomes the dominant signal.

For this imagery, microwave sounding data from the Advanced Microwave Sounding Unit (AMSU) aboard three NOAA polar orbiting satellites are used. More details on the satellite data are given in the next section.

# 3. AMSU

The Advanced Microwave Sounding Unit (AMSU) flies on the NOAA KLM satellites: NOAA 15, launched in 1998; NOAA 16, launched in 2000; and NOAA 17, launched in 2002, and is composed of a 48km resolution temperature sounder (AMSU-A) and a 17km resolution humidity sounder (AMSU-B). AMSU-A is a fifteen channel sounder with a frequency range of 23.8 - 89.0 GHz; AMSU-B has five channels ranging from 89.0 to 183.3 GHz. AMSU is part of a set of instruments known as ATOVS (Advanced TIROS Operational Vertical Sounder) which are used to obtain information about the vertical profiles of temperature and humidity in the atmosphere, which can then be assimilated into numerical atmospheric forecast models.

ATOVS data from the NOAA satellites is received via two methods:

- via the once per orbit data download from the spacecraft to the central NOAA station
- via direct broadcast from the satellite to individual ground stations

The first method of transmission provides global ATOVS/AMSU data, but with a delay of several hours after the time of measurement. Direct broadcast provides almost immediate data, but is limited to the region around the ground station.

The Special Sensor Microwave Imager Sounder (SSM/I(S)), operating on the US military DMSP satellites, is a 24-channel sounder which could also be exploited for this study in the same way as AMSU-A and AMSU-B. Adding SSM/I(S) would also provide more frequent updates than AMSU, although as SSM/I(S) data is not currently available by direct broadcast, only global (and therefore delayed) datasets would be available.

## 4. Eumetsat ATOVS Retransmission Service

The Eumetsat ATOVS Retransmission Service (EARS) was developed with the aim of providing sounder instrument data from the National Oceanic and Atmospheric Administration (NOAA) polar orbiting satellites with a coverage and timeliness suited to the needs of operational short range regional numerical weather prediction models. As mentioned above, the global ATOVS data that is received from NOAA arrives with a delay of 1.5-7 hours. Local area models (e.g., UK Mes) tend to have a data cut-off of about 1.5 hours, so no ATOVS data arrives in time to be used in the model runs.

EARS aims to address this problem by receiving direct broadcast data (which arrives to the user with a delay of only 10-20 minutes) from many ground stations and collating the data into a single file centrally at Eumetsat. The local data is currently collected from six stations including Tromso (Norway), Masapalomas (Canary Islands), Kangerlussuaq (Greenland) and Athens (Greece). The geographical coverage achieved by this network of stations is shown in Figure 1.

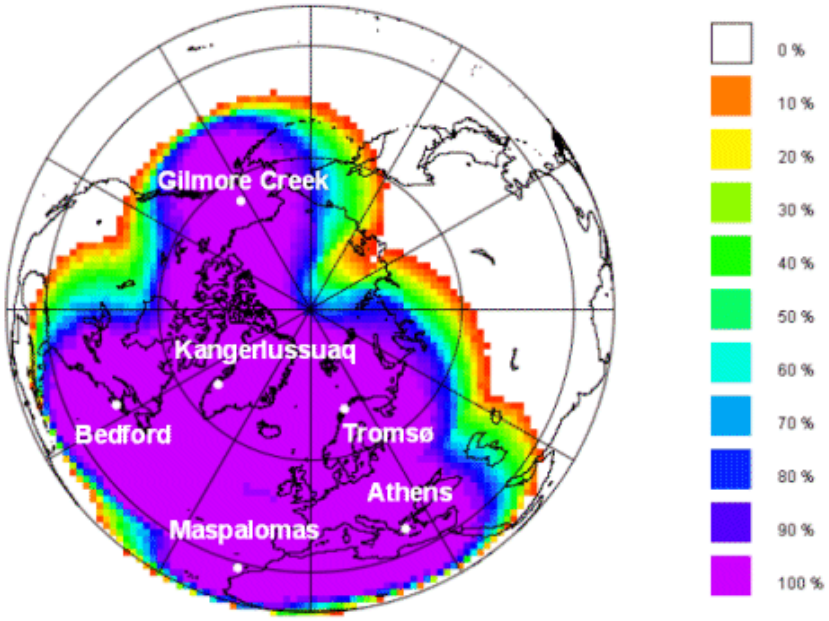


*Figure 1: Current coverage of EARS stations (taken from the EARS Technical Description 2004)*

Figure 2 indicates the frequency for the full coverage area, expressed as an average number of passes per day for a single satellite.

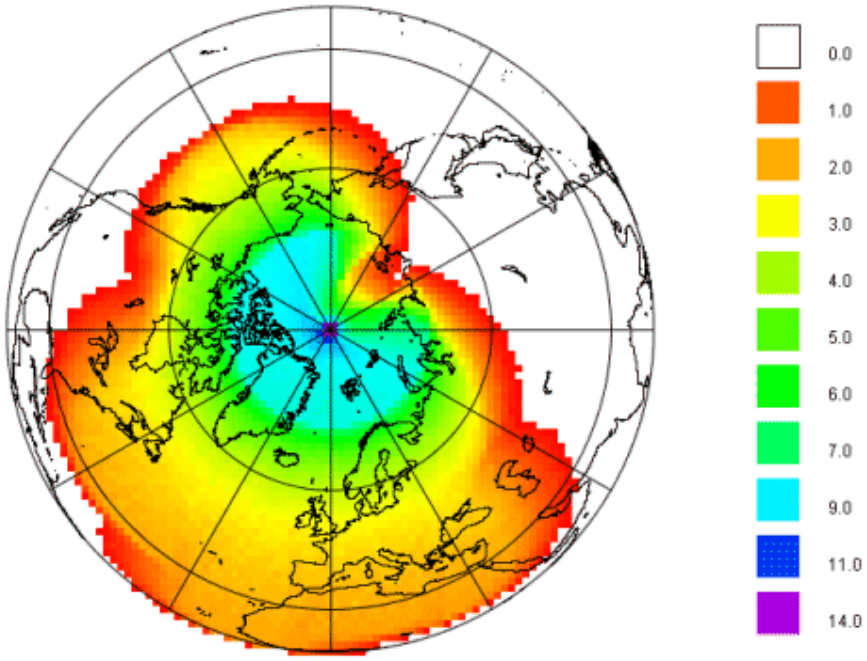


*Figure 2: Number of passes per day for a single satellite (taken from the EARS Technical Description 2004)*

## 5. Pre-Existing Imagery

This study has built on imagery techniques in place for direct broadcast ATOVS data over the UK area. This pre-existing ATOVS imagery product is made up of 3 components: a Meteosat IR image, an AMSU cloud liquid water index and an AMSU scattering index. An example image is shown in Figure 3.

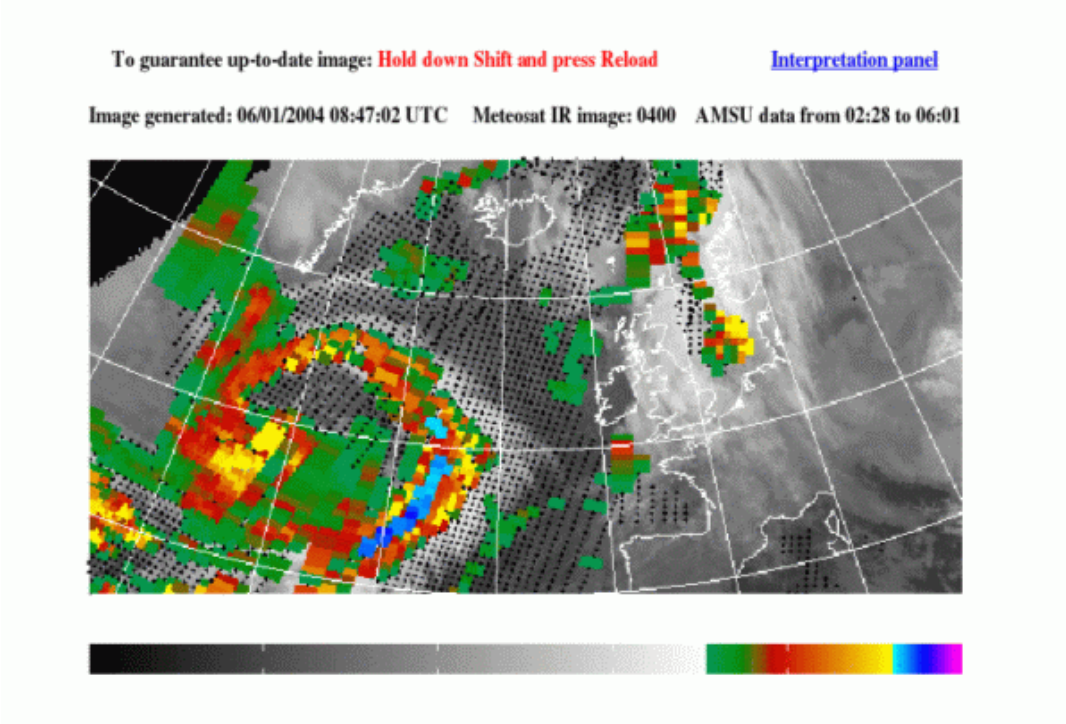


*Figure 3: Example of the pre-existing imagery*

The Meteosat IR component of the imagery (black/white colour scale) represents the infra-red image closest in time to the centre of the AMSU data window.

The AMSU cloud liquid water index (green to yellow colour scale) (Labrot *et al* 2005) strictly represents an inverse probability that the given AMSU field of view is cloud free. In practical terms, this translates to a higher index for a larger amount of liquid water within the satellite field of view. As the liquid water content increases, the probability of precipitation contributing to this signal increases. This technique relies on a low emissivity surface, so can only be applied over the ocean and some ice surfaces.

The AMSU scattering index (blue to pink colour scale) (Labrot *et al* 2005) will be discussed in the following chapters. In the pre-existing imagery shown here, it is only valid over water surfaces. However, the scattering index technique (unlike the cloud index) does not rely on a cold (i.e., ocean) surface, and can actually work better over surfaces with a high emissivity (i.e., land). The difficulty is in constructing imagery that will work equally well over all land surfaces (where the emissivity can be highly variable), and in treating coastal areas, surface water and snow- or ice-covered land.

# 6. Calculation of an All-Terrain Scattering Index

As mentioned above, the existing imagery is currently only produced over the ocean, due to the difficulty in interpretation of passive microwave data over land. The cloud liquid water index is still valid only over the ocean, due to its reliance on radiatively cold surfaces. However, recent work has made progress in allowing an all-terrain scattering index product. The following sections describe the algorithm that has been used to achieve this.

## *6.1. Channel Selection*

The channels employed in the derivation of an all-terrain scattering index are shown in Table 1. These channels were chosen due to their relatively low sensitivity to water vapour or oxygen absorption, allowing a more accurate retrieval of precipitation information.

| Satellite Characteristics | AMSU-A | AMSU-B |
|---|---|---|
| Spatial resolution | 3.3° | 1.1° |
| Nadir effective field of view | 50x50 $km^2$ | 20x16 $km^2$ |
| Scan edge effective field of view | 150x80 $km^2$ | 64x52 $km^2$ |
| Channels used | 23.8, 31.4, 89.0 GHz | 89.0, 150.0 GHz |

*Table 1: Characteristics of AMSU-A and AMSU-B instruments (taken from Goodrum et al (1999) and Bennartz (2000))*

At the lower frequencies (23.8GHz and 31.4GHz), emission from liquid precipitation dominates the signal, elevating the brightness temperatures measured by the satellite over surfaces with low emissivities (i.e., over the ocean). Over the land, surface emissivities are too high and variable for this signal to be reliable.

At higher frequencies (89GHz and 150GHz), the dominating signal is scattering by precipitation-sized ice particles, which acts to decrease the satellite-observed brightness temperatures. This signal is indirectly linked to surface precipitation. It can also be used reliably over both land and water surfaces. In the case of AMSU, another advantage of

employing these frequencies is the higher spatial resolution of AMSU-B, which will allow a more dynamic response to precipitation events, especially if the precipitation areal extent is small.

The first step in the algorithm is to make a distinction between land and water surfaces, and the subsequent processing of the AMSU data will differ depending on this. This determination of surface type is made within the ATOVS and AVHRR Processing Package (AAPP) (Labrot *et al* 2005) system and passed to the scattering index calculations.

The algorithm includes an offset value term representing the difference in the brightness temperatures at 89GHz and 150GHz. Currently, this is explicitly calculated over the ocean, using an average value of a local array of points. This is a very specific part of the algorithm as it is strongly dependent on the water vapour path and atmospheric temperature, and so can vary greatly depending on atmospheric conditions. Over land, the background is set to a constant. Details of the method are given in the following sections.

## 6.2. Land Surfaces

### *Snow and ice screening*

As discussed in Section 2, over land the surface emissivity is high and the signals from liquid cloud emission and surface emission are not easily distinguishable by satellite-observed brightness temperatures. Therefore precipitation identification is dependent on the scattering signal of precipitation-sized ice particles. At high frequencies, the signal from snow or ice cover on land surfaces is similar to that from frozen precipitation, leading to some ambiguity in the detection of precipitation. This is a potential problem with high, snow-covered mountains in the Middle East Crisis Area Mesoscale Model (CAMM) area. Therefore, a screening of snow- and ice- covered surfaces (based on the scheme of Grody et *al* (1999)) has been made available for implementation within the scattering index algorithm. This screening is a sequence of threshold tests on the brightness temperatures measured by AMSU-B 89GHz and 150GHz, and AMSU-A 23 and 31GHz channels. At present, the flagging appears to be excessive, and we are losing signals that may well be due to precipitation. Therefore, the screening is currently switched off, with the condition that users should be aware of possible false signals over snow-covered ground.

### *Identification of precipitation*

Following Bennartz et *al (*2002*)*, the identification of precipitation over land is based on the temperature difference between the 89GHz and 150GHz channels, allowing the use of full-resolution AMSU-B data. The scattering index over land, $si_{land}$, is calculated as shown in Equation 1.

$$si_{land} = (T_{89} - T_{150}) - (0.158 + 0.0163\theta) \qquad \text{Eq.1}$$

The brightness temperature at 89GHz is denoted by $T_{89}$; $T_{150}$ is the brightness temperature at 150GHz. The last term accounts for the dependence of the difference of the brightness temperatures on surface zenith angle, $\theta$.

## 6.3. Water Surfaces

### *Emission signal*

The emission signal in the lower frequency channels of AMSU-A can be used to derive the cloud liquid water index that was a feature of the original imagery. Currently, this is omitted

from the imagery in the CAMMS area due to the high proportion of land surface over water in this area (as mentioned above, this indicator is valid only over the ocean). However, we would be interested in feedback from users on this matter, and a cloud water index over the water could be reinstated if desired.

***Scattering signal***

Bennartz et *al* (2002) investigated the use of several pairs of window channels, in the same way as for land surfaces, for obtaining scattering indices over water. It was concluded that a pairing of 89 GHz and 150 GHz was optimal, with the added advantage of having both channels at AMSU-B resolution.

For AMSU-B fields of view over the ocean, the scattering index, $si_{ocean}$, can be calculated as shown in Equation 2.

$$si_{ocean} = (T_{89} - T_{150}) - (ave\_back\_sea + 0.1104\theta) \qquad \text{Eq.2}$$

Again, $\theta$ *is* the surface zenith angle in degrees, $T_{89}$ is the brightness temperature at 89GHz and $T_{150}$ is the brightness temperature at 150GHz. The term *ave_back_sea* represents the background (average) offset between $T_{89}$ and $T_{150}$ over water, which is considerable. Bennartz et *al* (2002) used a constant value (-39.2010K) derived from their test data sets, but recommended the explicit calculation of this term to account for the strong dependence on atmospheric conditions (e.g. water vapour path). Section 9 presents results using both the constant value and explicitly calculated values to calculate the scattering index over water surfaces.

# 7. Interpretation of New Imagery

The ATOVS imagery product is made up of 2 components: a Meteosat IR image and an AMSU multi-channel composite image.

## *Meteosat IR Component*

This component of the imagery (black/white colour scale) represents the IR image closest in time to the centre of the AMSU data window.

## *AMSU Scattering Index*

Microwave measurements detect precipitation-sized ice hydrometeors. Therefore, unlike infrared measurements they only respond to ice cloud associated with precipitation. Infrared measurements respond to any high ice cloud. The imagery shows how large the impact of precipitation-sized ice hydrometeors is through a multi-channel index called the "scattering index". The higher the value of the scattering index the more numerous and larger the ice hydrometeors. Therefore, increasing values of the scattering index are a much more reliable indicator of rain than cloud top temperature. However this technique will not identify rain whose processes do not require an ice phase, e.g. drizzle from marine stratocumulus. However these warm rain processes are unlikely to be associated with severe weather likely to cause disruption.

# 8. Example Image

An example image is shown in Figure 4. This example is from 12/08/04 and depicts a cut off low over the UK and north-west Europe with associated deep convection.

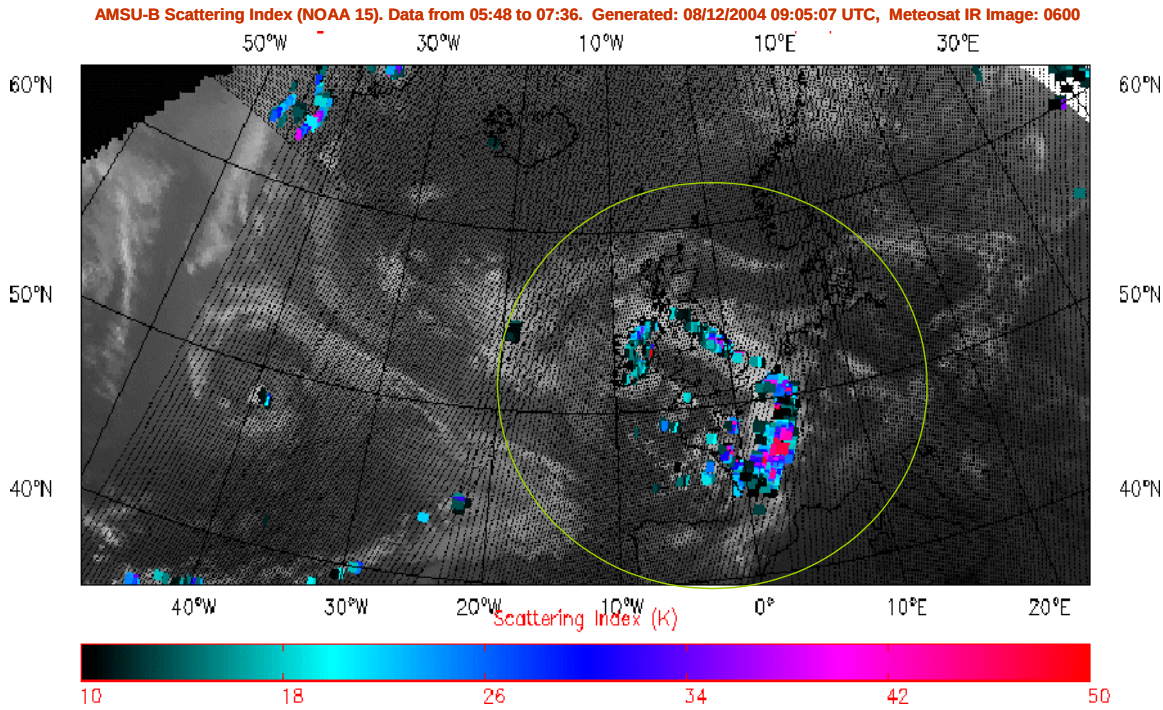


*Figure 4: Example image over the UK and North Atlantic area*

The image title provides information on which NOAA satellite provided the data, the period of time over which the AMSU-B scattering index data is available, the time of generation of the image, and the time of the Meteosat IR image.

The colour bar denotes the range of values of the scattering index in degrees Kelvin. The range from 10K to 50K was chosen to optimize the benefits of the scattering index by only plotting significant scattering. The higher the value of the index, the more precipitation is identified.

The black dots indicate fields of view of the satellite pass where the scattering index was below the threshold.

Figure 5a shows a blown up view of the rough area circled in Figure 4. Figure 5b is the corresponding IR-only image. The radar image (at 06:30) is shown in Figure 5c.

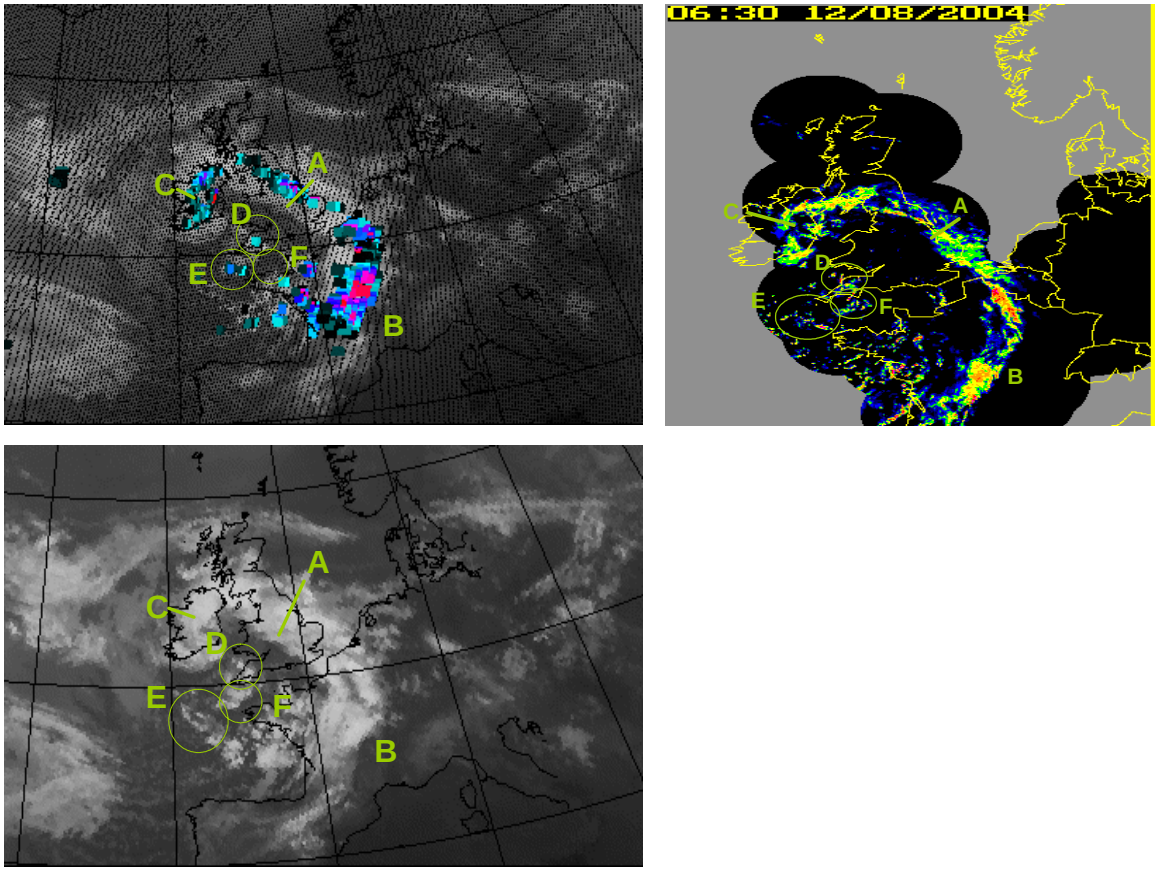


*Figures 5a(top left): the scattering index image derived from data from 0548 to 0736 , 5b(bottom left): corresponding IR image, 5c(top right): Nimrod radar image at 0630.*

**A-C**: Frontal Precipitation:

Both the areal extent and the intensity of the frontal precipitation shown by the radar are captured well by the scattering index imagery.

In the IR image, the southern-most boundary of the high cloud band stretches in a line from Brighton, through the Midlands to Anglesey (the band marked as **A**). In the scattering index imagery, the precipitation boundary is over 150 km north of the edge of the cloud band, agreeing with the radar, and more accurately indicating the areas of strong precipitation.

The variations in intensity along the front as shown on the scattering index imagery also agree well with the radar image, for example at **B**. These areas of higher and lower intensity are not easily identifiable from the IR image alone.

Both the radar image and the composite image identify an area over central-eastern Ireland where no precipitation is present (**C).** The IR-only image shows continuous high cloud over this area, and there can be no distinction between the precipitating and non-precipitating regions.

**D-F**: Areas of strong convection:

Three areas of strong convection are identifiable on the radar image: one over south-west England (**D**) and two over the English Channel (**E-F**). The convection over south-west England is shown up on the scattering index imagery, as is the more westerly of the two convective areas over the Channel (**E**). The third convective area (**F**) is missed by the scattering index. This is due to the resolution of AMSU-B (17-35km); no features smaller than this can be reliably resolved. Radar has a much finer resolution and so can pick out these

features. Convection over north-west France is also identifiable in the scattering index imagery.

# 9. Validation of the Imagery over the UK

An evaluation of the scattering imagery can be made over the UK area where corresponding radar data is available for comparison. For this study, Met Office Nimrod European composite data on a 5km resolution grid, covering the UK and northern parts of western mainland Europe, were used. These data files are available every 15 minutes and include information on instantaneous rain rate, which should have a direct correlation to the scattering index, which indicates the probability of precipitation. In order to allow a more accurate comparison between the two data fields, the radar data were averaged to the AMSU-B data grid, which has a resolution of 17km. The mapping used in this study is not optimal but an optimal convolution scheme is not currently in place. The current averaging will become more inaccurate towards the edge of the satellite scan, where the distance between satellite grid points increases.

## *9.1. Qualitative Validation against Radar Data*

An initial evaluation of the scattering index imagery was carried out by a qualitative comparison to radar data over the UK area, using Met Office Nimrod European composite data.

Figure 6 shows a comparison of radar rain rate with the AMSU scattering index for one case study, showing a mature low pressure to the west of the UK on 22 June 2004 The satellite pass data ranges from 1402 to 1408, and the radar data is at 1400. It can be seen that, while the scattering index algorithm is capable of producing a qualitative match to the radar rain rate over land, in terms of spatial extent and relative intensity (except for some convective features over mainland Europe, where the resolution of the AMSU-B instrument is perhaps too coarse to reliably resolve them), over water surfaces the signal is too weak. This discrepancy is due to the method of calculation of the difference between brightness temperatures at 89GHz and 150GHz, which is used to calculate a background value. Bennartz et *al*. (2002) stressed that this offset over water is the most atmospherically dependent part of the algorithms as it is strongly dependent on atmospheric water vapour path and temperature.

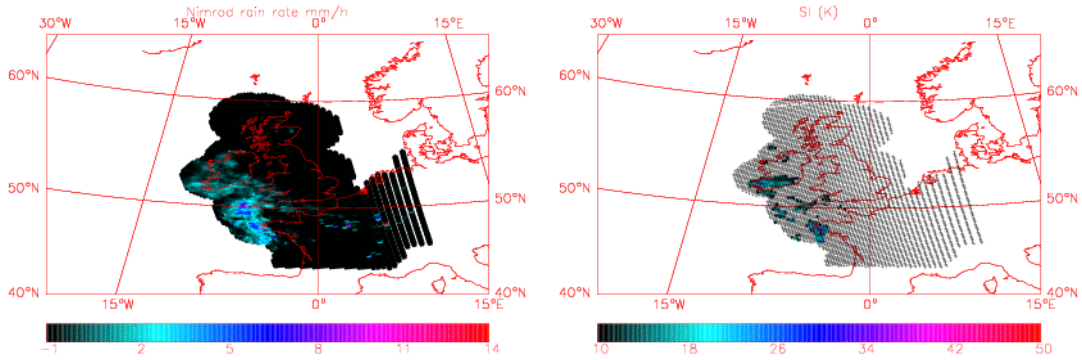


*Figures 6a (left): Nimrod radar rain rate data at 1400 on 22/06/04, convolved to the AMSU-B grid; Figure 6b (right): scattering index derived from AMSU-B data from 1402 to 1408, using a local array of sea points to calculate the average brightness temperature difference*

The background brightness temperature offset was calculated using a local array of sea points. In order to try to improve the match over water surfaces, other methods were also trialled; using a constant value (from Bennartz et *al*), and using the average value of all sea

points in the domain (rather than a local array). The results from these methods can be seen in Figure 7.

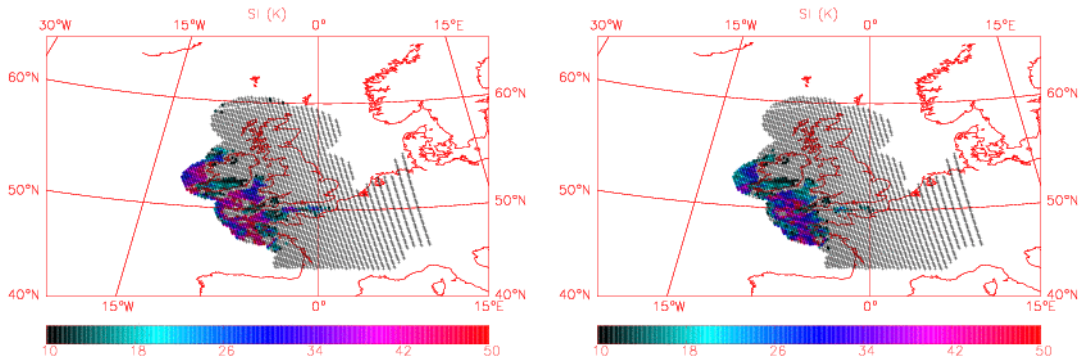


*Figure 7a(left) : As Figure 6b, but using a constant value for the background temperature difference, and Figure 7b: Using an average value calculated from all the sea points*

These methods do now pick out the area of heaviest rainfall but are also over-estimating the extent of the rainfall to the west of Ireland compared with the Nimrod radar data.

Figure 8 shows another case study, from 14 December 2004, where the Nimrod data shows precipitation associated with a cold front over Ireland and Scotland. The satellite data is from 0420 to 0426 and the radar data is an instantaneous value at 0430.Again the scattering index picks up the areas of precipitation over the land, and also shows up areas of scattering to the east of Scotland and over the Irish sea, where the radar shows precipitation. However, areas of precipitation over water to the west of Ireland and to the north of Scotland are not picked out.

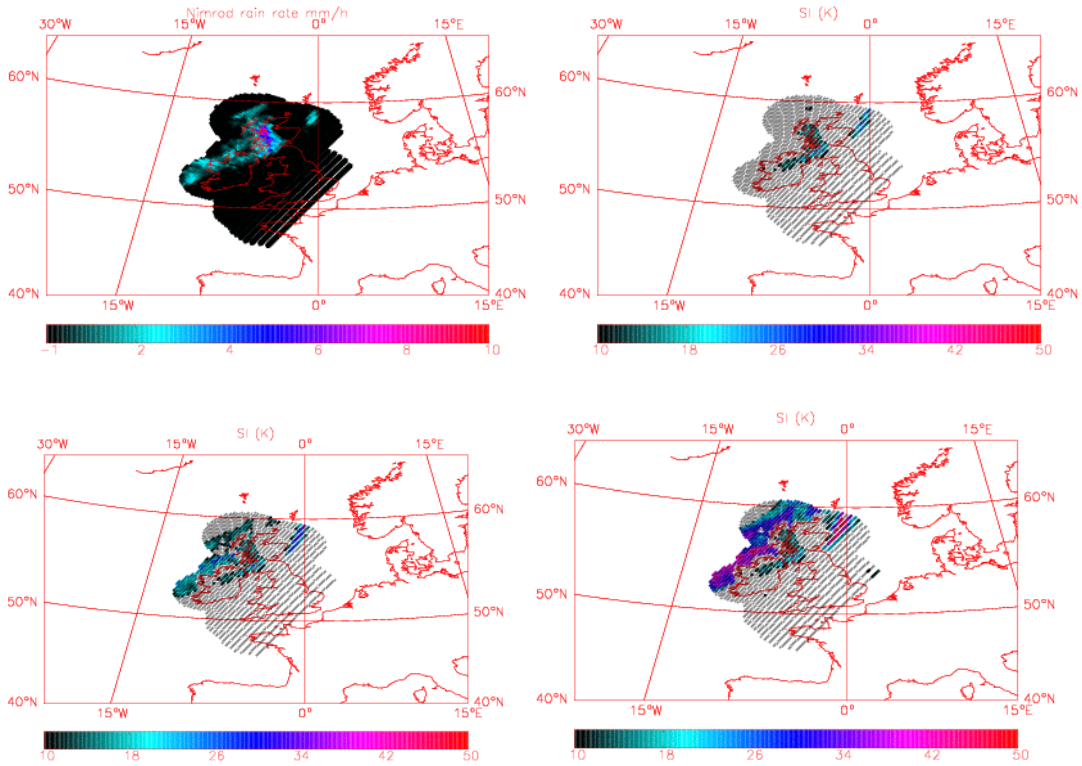


*Figure 8a (top left): Nimrod radar rain rate at 0430 on 14/12/04, Figure 8b (top right): scattering index derived from AMSU-B data from 0420 to 0426 using a local array of sea*

*points to calculate the average background brightness temperature difference, Figure 8c (bottom left): As 8b but using an array of all sea points, Figure 8d (bottom right): as 8b but using a constant background brightness temperature difference.*

Again, Figure 8 shows that using a constant value or an average of all sea points, the algorithm is better able to identify the areas of rainfall to the west of Ireland and to the north of Scotland, but, especially in the case of using a constant value, tends to overestimate both the areal extent and the intensity when compared with radar.

In deciding on which method to use, it was decided to reject using a constant value for the background brightness temperature difference over the sea, even if it could be tuned for this data set to give good agreement with radar data. This is because, as mentioned earlier, this difference is very sensitive to atmospheric conditions, such as water vapour path and temperature, and a constant value would be unable to represent this. This is especially true since we are producing the imagery for domains where the atmospheric conditions are very different to the UK, such as the Middle East.

As the method using a local array of points to calculate the background was underestimating the precipitation over the sea compared to radar, and using all the sea points was producing an overestimation, it was decided to enlarge the extent of the local array used to a grid of 5°x5°. Figures 9 and 10 show the results of implementing this in the algorithm for the two case studies shown above.

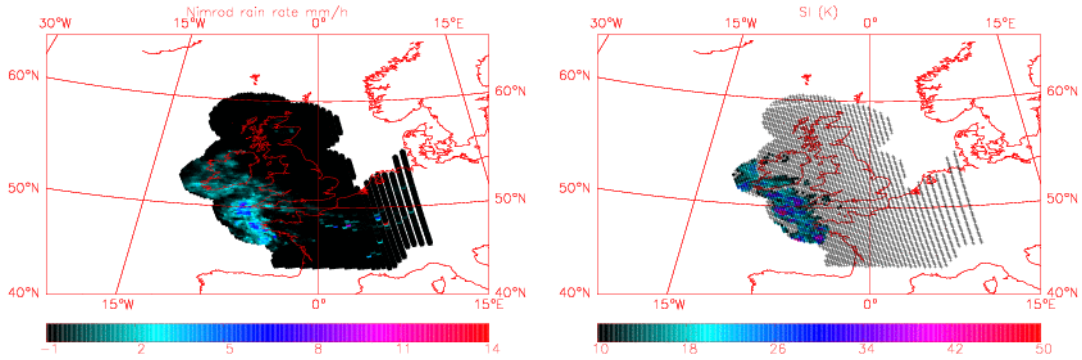


*Figure 9a (left): Nimrod radar rain rate data at 1400 on 22/06/04 , convolved to the AMSU-B grid; Figure 9b (right): Scattering index calculated using an extended array of local sea points to calculate an average background brightness temperature value.*

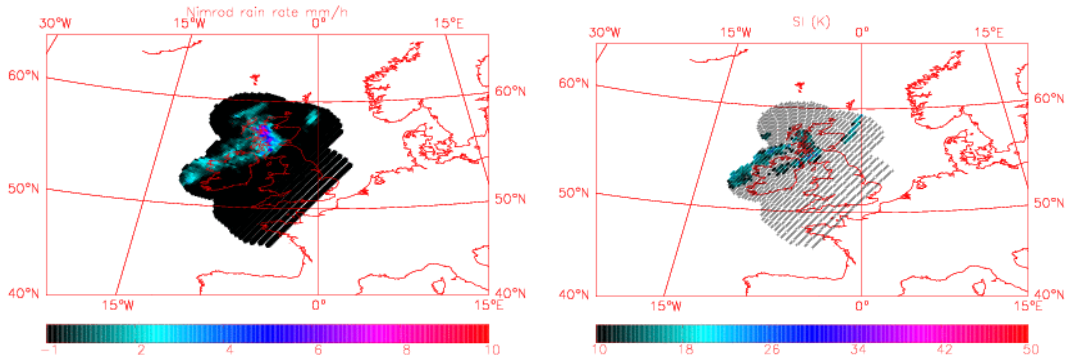


*Figure 10a (left): Nimrod radar rain rate data at 0430 on 14/12/04 , convolved to the AMSU-B grid; Figure 10b (right): Scattering index calculated using an extended array of local sea points to calculate an average background brightness temperature value.*

This method appears to give the closest match between radar data and the scattering index.

### *9.2. Quantitative Evaluation against Radar Data*

The qualitative evaluation in Section 3.1 indicated that the method of calculating the background brightness temperature offset which gives the closest qualitative match to the corresponding radar data is using the mean value from an extended array of local sea points. A quantitative evaluation has been carried out between the scattering index data derived using that method and the Nimrod rain rate data.

The evaluation was carried out for 19 case studies, ranging in date from June 2004 to February 2005. As the scattering index data represents a probability of precipitation rather than an actual precipitation rate, the quantitative evaluation is based on the ability of the index to represent four rain rate classes, which are defined from the convolved rain rate data. These classes are show in Table 2.

| Class | Description | Minimum rain rate (mm/h) | Maximum rain rate(mm/h) |
|---|---|---|---|
| **1** | No rain | 0.0 | 0.1 |
| **2** | Risk of light rain | 0.1 | 0.5 |
| **3** | Light to moderate rain | 0.5 | 5.0 |
| **4** | Heavy rain | 5.0 | ∞ |

*Table 2: Classification of precipitation intensities*

Figures 11a and 11b are histograms showing the distribution of the scattering index for the four rain rate classes. The histograms have been normalised by the number of data points in each class in order to give a representation of the prior probability of the rain rate class occurring as well as the probability of a given scattering index belonging to that class. Figure 11a show the results for data points over water surfaces, and Figure 11b is for land surface points.

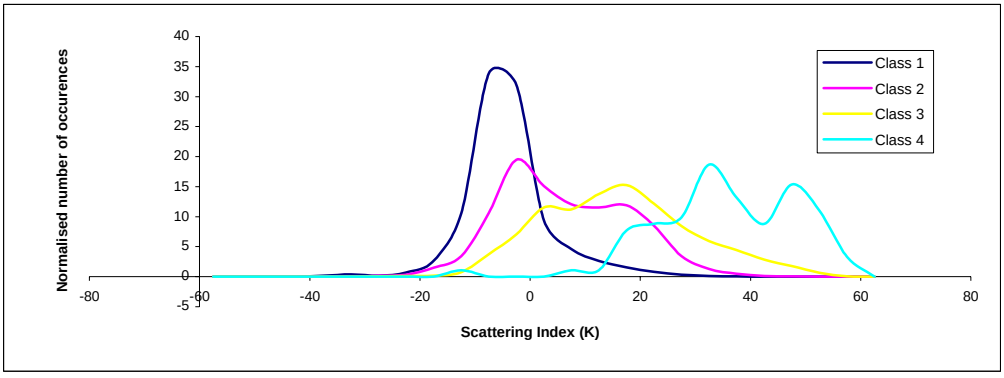


*Figure 11a (above): Histograms (normalised by the number of elements in each class) showing the distribution of the scattering index for the four rain rate classifications, for sea points*

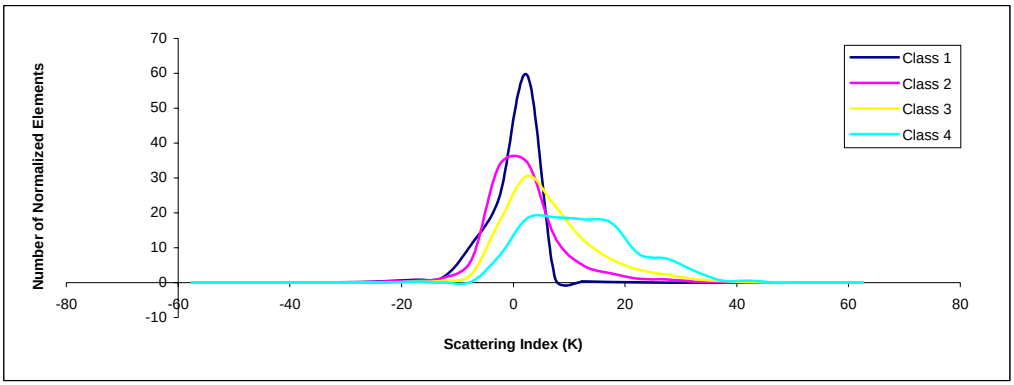


*Figure 11b: As Figure 11a but for land points*

It can be seen from Figures 11a,b that the separability of the classes over water surfaces is greater than for over land. Over land, Figure 11b suggests that only Class 4 (heavy precipitation) would be separable in practice. It might have been expected that there would be a stronger sensitivity to the precipitation (and thus greater separability between the classes) over land, where the satellite is sensing scattering from a cold atmosphere over a warm surface. However, more ambiguity may arise due to the high variability of the surface. The signal also saturates more quickly over the land, with few pixels having a greater scattering index than 40K. This effect can be seen in Figure 12, which shows the change in scattering index calculated from modelled radiances with ice water path for land and sea fields of view (which is correlated to precipitation).

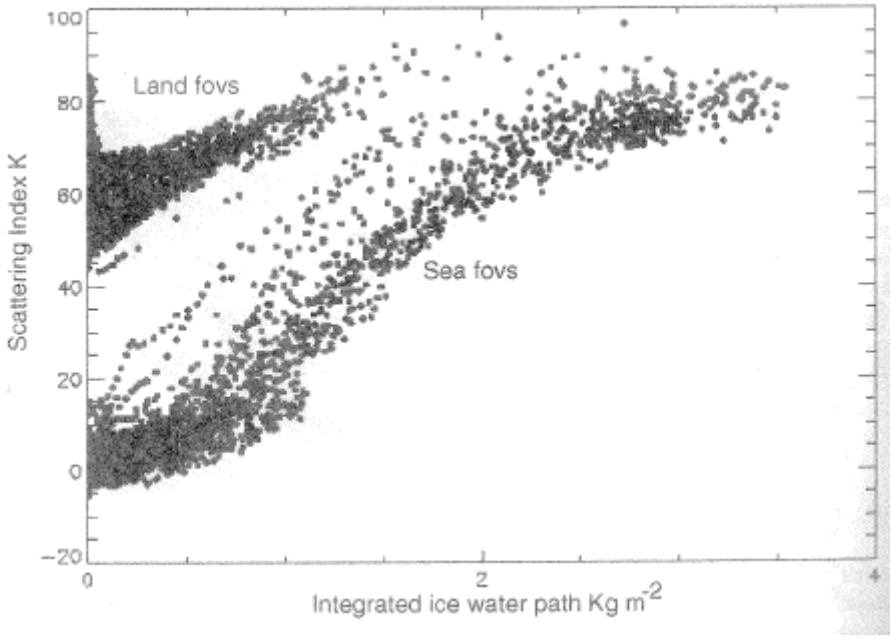


*Figure 12: The change of scattering index with ice water path for land and sea field of views (fovs) (from English et al. 1997).*

Differences may also arise due to the fact that the spatial scales of convection are much greater over water than land, and therefore the inaccuracies introduced by the sub-optimal mapping that is currently implemented may have more effect on land points.

A probability of a given scattering index belonging to a certain class can be derived by normalising the histograms to a peak value of 1 and imposing the constraint that for each

scattering index the total probability has to equal 100%. The resulting probability graphs are shown in Figures 13a (water) and 13b (land).

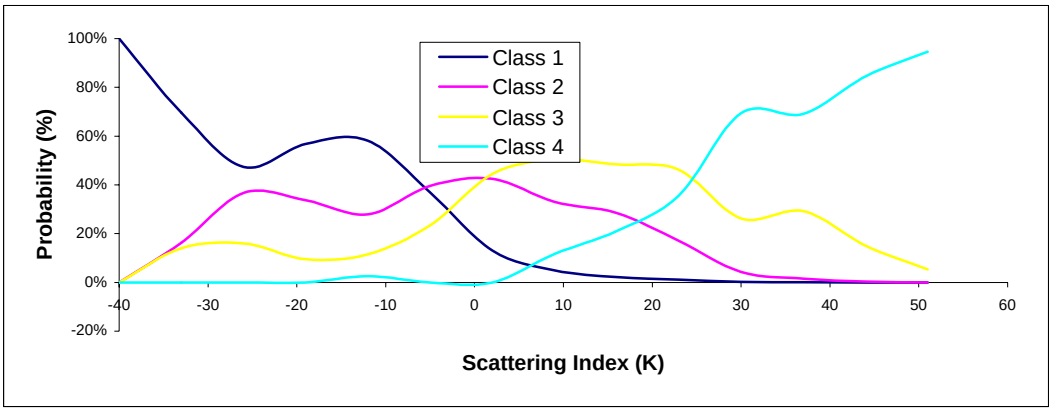


*Figure 13a: Probability of a given scattering index belonging to each rain rate class, for water points*

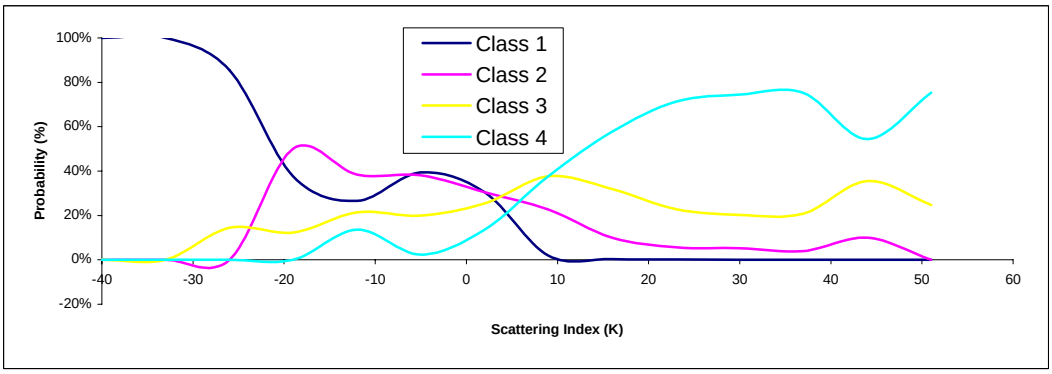


*Figure 13b: As for Figure 13a but for land points*

The probabilities shown in Figures 13a,b indicate the probability of a given scattering index being in each class, with no prior knowledge of the probability of that class of rain rate occurring. For example, for a scattering index of about -3 over the sea, the probability graph suggest that classes 1 and 3 are equally likely with a probability of the scattering index being in those classes at about 25%. The probability of class 2 is slightly higher at about 40%. However, Figures 11a,b, which shows the distribution of the scattering index data set normalised by the number of elements in each class, indicates that for this value of the scattering index, far more data points belonged in Class 1, because a rain rate belonging in Class 1 occurred many more times than for the other classes. Therefore, care must be taken to distinguish between an absolute probability, with no prior knowledge of the likelihood of that rain rate class occurring, and a conditional probability which takes that likelihood into account.

A contingency table was derived for the four classes by choosing thresholds between the classes that forced the climatology to match the distribution of rain rate data, thus imposing the prior knowledge of the likelihood of each class occurring. For the data used in this study, the thresholds between the classes were found to be roughly -3K, 10K, 26K for sea points and -0.25K, 2K and 9K for land points (i.e. the threshold between Class 1 and Class2 over the ocean is approximately -3K). The contingency tables for pixels with sea and land field of views are shown in Table 3a and 3b respectively.

| | Classified as (%) | | | | |
|---|---|---|---|---|---|
| Belongs to | Class 1 | Class 2 | Class 3 | Class 4 | No. of data points |
| Class 1 | 64.13 | 30.37 | 5.08 | 0.40 | 15767 |
| Class 2 | 22.33 | 40.32 | 32.42 | 4.91 | 1545 |
| Class 3 | 6.98 | 27.65 | 43.59 | 21.75 | 2289 |
| Class 4 | 1.09 | 1.09 | 21.97 | 75.82 | 91 |

*Table 3a: Contingency table for the four rain rate classifications over the sea*

| | Classified as (%) | | | | |
|---|---|---|---|---|---|
| Belongs to | Class 1 | Class 2 | Class 3 | Class 4 | No. of data points |
| Class 1 | 34.22 | 61.48 | 3.73 | 0.57 | 45623 |
| Class 2 | 40.48 | 18.21 | 29.67 | 11.62 | 3690 |
| Class 3 | 19.55 | 14.28 | 36.11 | 30.03 | 5706 |
| Class 4 | 7.39 | 5.86 | 28.57 | 58.16 | 392 |

*Table 3b: Contingency table for the four rain rate classifications over the land*

The results for the water points indicate that a clear separability exists between the four rain rate classes. Only about 5.5% of precipitation-free pixels are falsely classified as moderately to heavily precipitating (5.08% in class 3 and 0.4 % in class 4). Equally for heavy precipitation, only about 1% of pixels are classified as rain free, indicating a good separability between non-precipitating and heavily precipitating classes.

Over land, the mismatch between the verification classes and observation classes is not so good, especially for low rain rates. This may be due to the difficulty of this type of quantitative evaluation rather than an indication of the ability of the scattering index calculation method. It is also possible that an optimal convolution may improve these results, for the reasons stated earlier. Nevertheless, the contingency table still show a strong separability between heavy precipitation and no/light precipitation, despite the difficulties in verification.

### *9.3. Application to Other Domains*

A list of domains existing at the time of project completion is given in Section 13.

Bennartz et *al*. (2002) stressed that the brightness temperature offset between 89GHz and 150GHz, which is used in the calculation of the scattering index over water surfaces, is strongly dependent on the atmospheric conditions. Using the same constant value for the brightness temperature offset in, for example, the Middle East, as in the mid-latitudes is likely to give erroneous results. Figure 14 is an example of the variation of the response of 89GHz and 150GHz over water surfaces with latitude. As the water vapour path is highly correlated to latitude, this also gives an indication of the variation against water vapour.

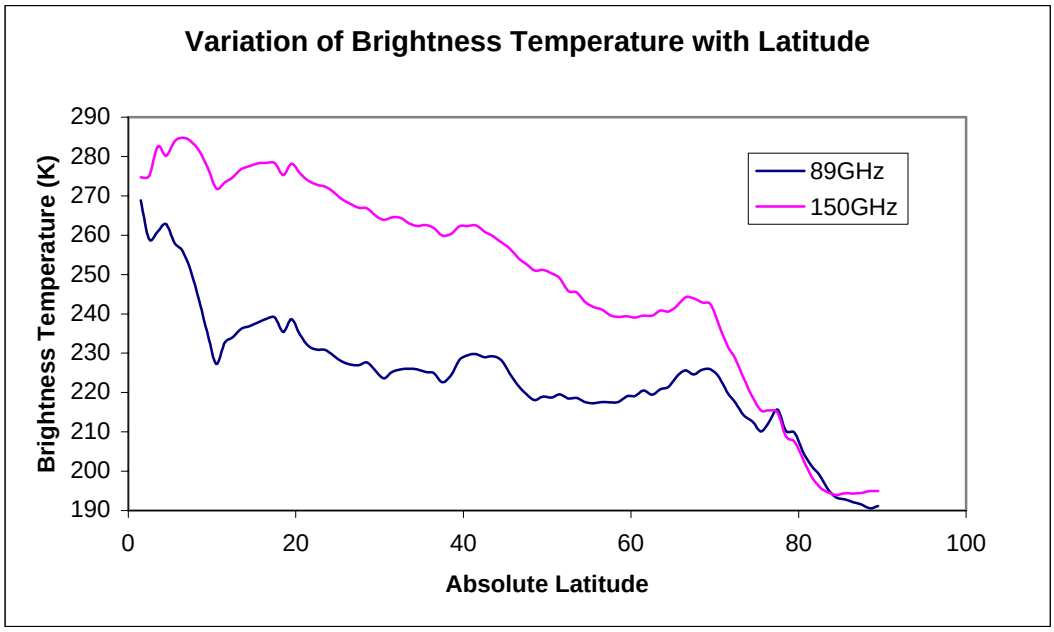


*Figure 14: The variation of brightness temperature with latitude for one day's worth of AMSU-B data (for data over water surfaces)*

Using the mean value of this offset over an array of the sea points in the domain, however, as opposed to using a fixed value, should implicitly account for this strong dependence. Figure 15 is a demonstration of these methods over the Middle East Crisis Area Mesoscale Model domain, for a case study on 21 November 2004. Figure 15a is the IR image at 0100. Figure 15b shows the scattering index derived from NOAA-15 AMSU-B satellite data from 2351 to 0139, where the brightness temperature offset over the water was calculated using a local array of sea points.

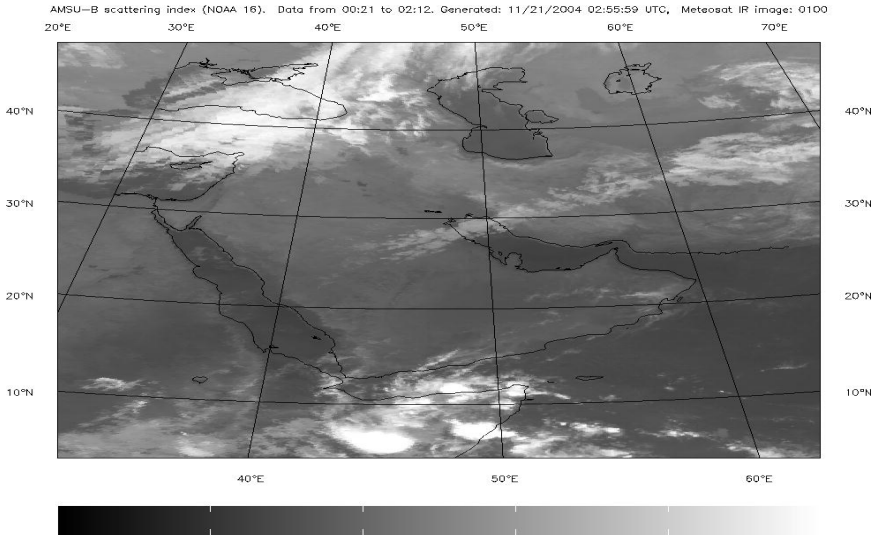


*Figure 15a: Infra-red image at 0100 on 21/1//04 over the Middle East Crisis Area Mesoscale Model domain*

Although there is no radar data for comparison, it can be seen there is a sharp contrast evident between the intensity of the scattering index over the land and sea, which is unlikely to be realistic. Similarly to the UK cases above, the precipitation signal seems to be underestimated over water surfaces. Implementing an extended local array gives a much smoother transition between land and water surfaces (Figure 15c)

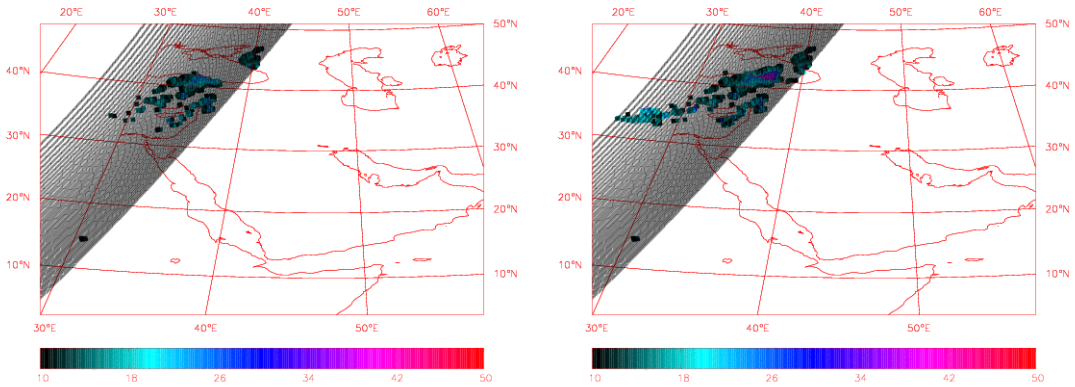


*Figure 15b (left): AMSU-B derived scattering index using data from 2351 to 0139, using a local array of sea data points to calculate the background brightness temperature difference, and Figure 15c: as Figure 15b but using an extended array of local sea points*

## 10. Scattering Index/Rain Rate Relationship

The scattering index that is plotted in these images is a value that represents the amount of scattering of microwave data away from the viewing satellite. The amount of scattering is strongly correlated to the amount of large ice crystals (and to a lesser extent, large raindrops) present in the field of view, which in turn is correlated to the probability of precipitation. Therefore, the scattering index is a measure of the likelihood of precipitation rather than an estimate of a rain rate. However, the stronger the scattering, the more large ice crystals, and so the higher the probability of a high rain rate, allowing a broad relationship to be defined between the scattering index and the rain rate. This relationship can be implemented based on the thresholds used to calculate the contingency tables above.

## 11. Timeliness and Frequency of Images

The EUMETSAT ATOVS Retransmission Service (EARS) was developed with the aim of providing sounder instrument data from the National Oceanic and Atmospheric Administration (NOAA) polar orbiting satellites with a timeliness suited to the needs of operational short range regional numerical weather prediction models. EARS receives direct broadcast data from many ground stations and collates the data into a single file centrally at Eumetsat. The Middle East Crisis Area Mesoscale Model domain is covered by data from the Athens ground station, and of course from global data (with a longer delay).

Data from Athens is currently available approximately 30 minutes after observation time. Observations at the Athens ground station occur whenever NOAA-15, NOAA-16 or NOAA-17 satellites fly overhead – about every two hours. Therefore, the images are currently generated every two hours. The time of generation was chosen to produce images as soon as possible after receiving the data, and should never be more than two hours after the observation time, assuming that the new Athens data has been received.

The generation of images is dependent on the timely reception of data from the Athens ground station. It should be noted that EARS is still in the development stage and outages or delays in the Athens data are possible.

# 12. Strengths and Weaknesses of the Imagery

### *Strengths*

- The ability to provide information on precipitation in areas not covered by a radar network.
- The directness of the relationship of the scattering index to precipitation: As mentioned earlier, the microwave frequencies can penetrate through the cloud top and interact with ice phase precipitation. Previous IR methods, which relate precipitation to cloud top height, are much more indirect methods of precipitation identification.
- The timeliness of the data
- The similarity of the imagery to radar data

### *Weaknesses*

- **Snow/Ice**: Over land, the signal from dry snow or ice cover is similar to that of frozen precipitation, leading to some ambiguity in the detection of precipitation. This is a potential problem with high, snow-covered mountains in the CAMMS area. A screening of snow- and ice- covered surfaces has been developed, but preliminary results indicate that the screening currently also removes much of the authentic precipitation signal. Until this can be tuned to remove signal from snow and ice while keeping all important information about the precipitation, it is omitted from the algorithm.
- **Dust Storms**: The effects of dust storms on the scattering signal are not yet well understood, and users should be aware of the possibility of the scattering index being triggered in these areas in the absence of precipitation.
- The resolution, which varies from 17km to 35 km across the satellite scan. Convection takes place on scales of less than 10km and so may not be fully resolved by the scattering index algorithm.
- The inability of this technique to identify 'warm' rain processes.
- The frequency of the images, which is constrained by the number of passes per day of the satellites over the Athens ground station.

# 13. Current Domains

The scattering index has been set up over several domains. Figure 5 showed the current domain over the UK area. This has also been extended to cover more of mainland Europe in a European domain – an example is shown in Figure 16.

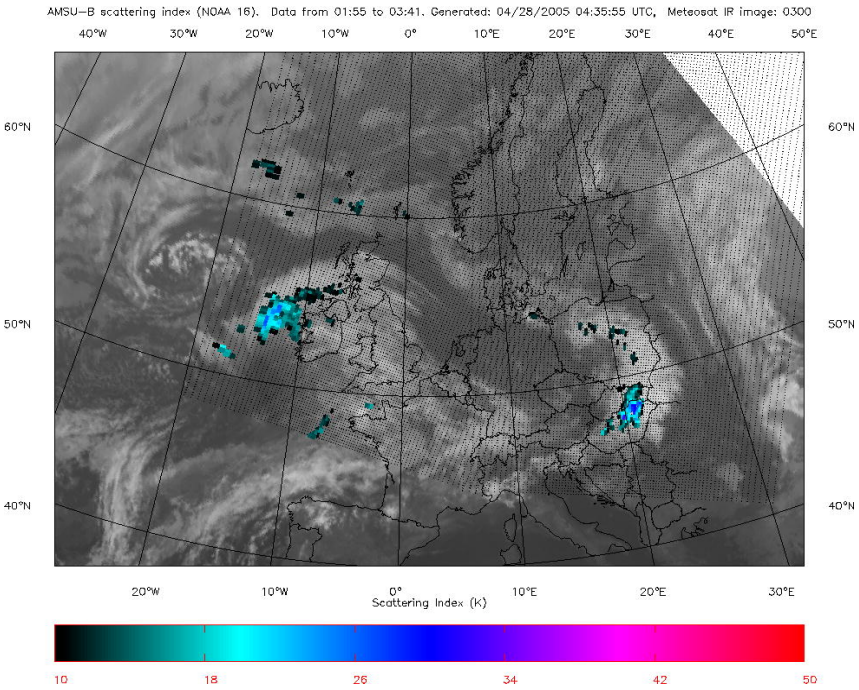


*Figure 16: Example of the imagery over Europe*

At the time of project completion, Crisis Area Mesoscale Model domains included the Middle East CAMM and the South West Asia CAMM. The Middle East CAMM is also covered by the composite imagery, as can be seen in Figure 17.

Again, Figure 17 demonstrates the advantage of the AMSU-B derived scattering index over IR-only imagery in picking up specific areas of strong precipitation beneath high cloud.

An example image of the scattering index imagery over the South West Asia CAMM domain is shown in Figure 18. Over this domain, suitable background IR imagery was currently unavailable at the time of project completion – the area was not covered by a single Autosat IR product, and so the microwave-based scattering index only is plotted.

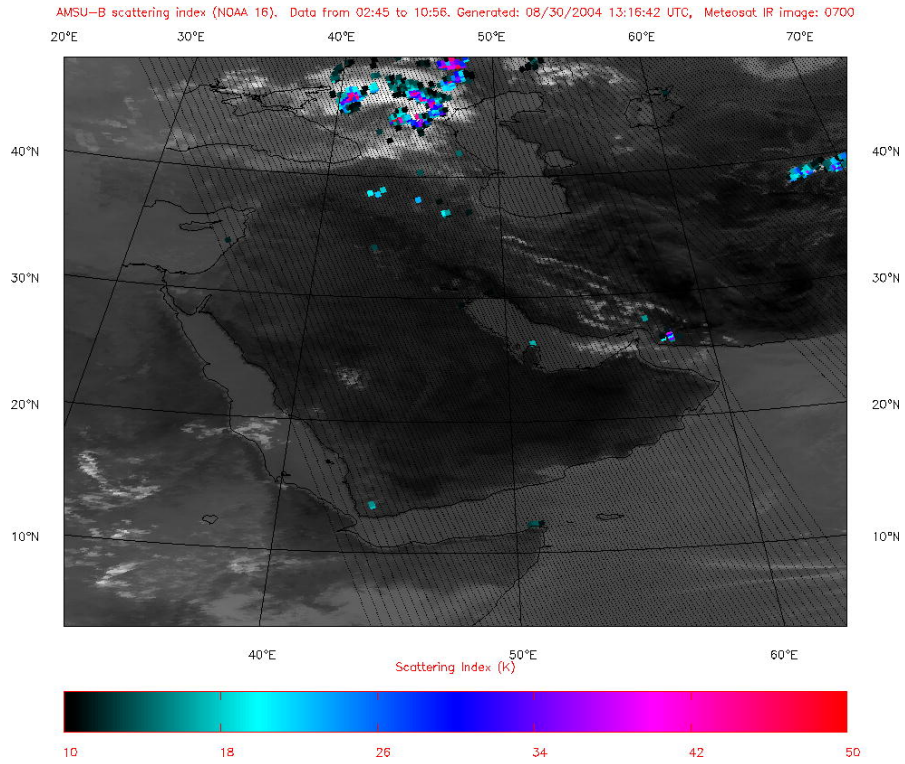


*Figure 17: Example composite image over the Middle East CAMM domain*

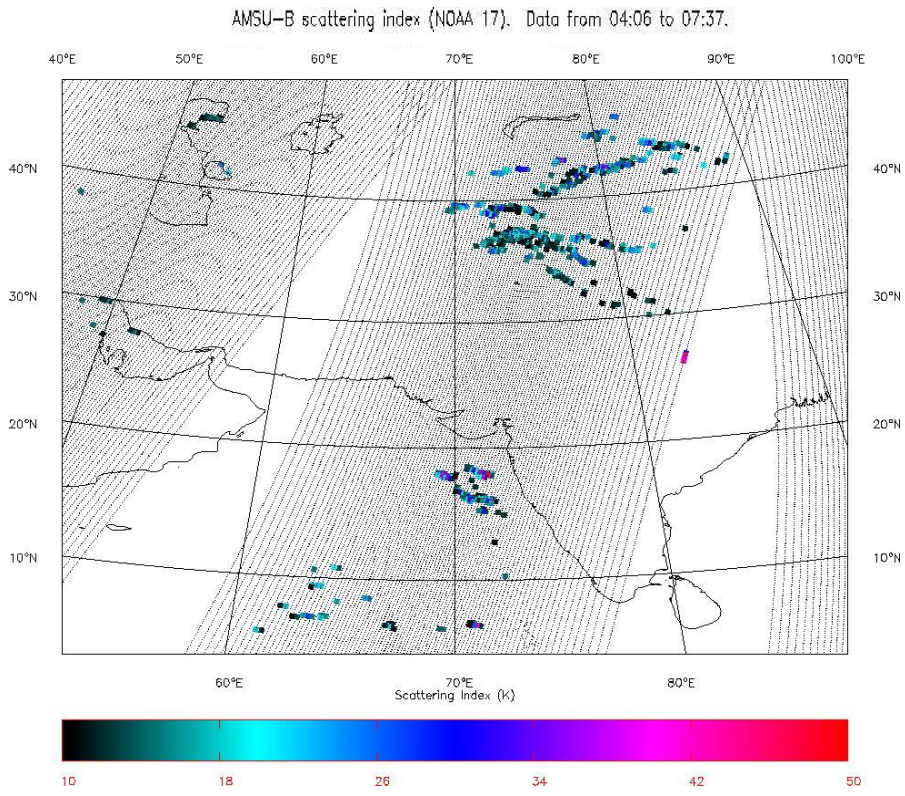


*Figure 18: Example image over the SW Asia CAMM domain(suitable background IR image not currently available)*

## 14. User Feedback

Feedback is actively sought from users on ways in which to improve the images in terms of quality and applicability for nowcasting and/or model verification. Feedback would be appreciated on the issue of snow and ice screening – is it preferable to leave in dubious signal from high, snow-covered mountains, with a warning for the user to be aware of this effect, and retain all information on precipitation, or to introduce the flagging, risking losing some of the real precipitation signal?

Feedback can currently be sent to *una.okeeffe@metoffice.gov.uk*

## 15. Acknowledgements

Thanks to Stephen English, Dave Jones, Perry Roe, Ian Brown and Stephen Moseley.

## 16. References and Further Reading

Bennartz, R., 2000, Optimal convolution of AMSU-B to AMSU-A. J. Atmos. Oceanic Technol, 16: 417-431

Bennartz R., A. Thoss and D.B.Michelson, 2002, Precipitation Analysis using the Advanced Microwave Sounding Unit in Support of Nowcasting Applications. Meteorol. Appl. 9, 177-189

English, S.J., R.J. Renshaw, P.C. Dibben and J.R. Eyre, 1997. The AAPP module for identifying precipitation, ice cloud, liquid water and surface type on the AMSU-A grid in Technical Proceedings of the 9th International TOVS Study Conference, Igls, Austria, February 1997 ; Ed.: J.R. Eyre; Published by ECMWF, Reading, UK; 119-139

Goodrum, G., K.B. Kidwell and W. Winston (eds.), 1999, NOAA KLM User Guide, U.S. Dep. of Commerce., NOAA/NESDIS/NCDC, Suitland, Maryland, USA, available at: http://www.nesdis.noaa.gov

Grody, N. C., F. Weng and R. Ferraro, 1999, Application of AMSU for obtaining hydrological parameters. In Proc. of the Fourth Conference on Microwave Radiometry, USP Int. Science Publishers, Florence, Italy, March 1999, 339-352.

Labrot, T., L. Lavanant, K. Whyte, N. Atkinson. P. Brunel, 2005, AAPP Documentation - Scientific Description Version 5.0 , Satellite Application Facility for Numerical Weather Prediction Document NWPSAF-MF-UD-001, available from the NWP SAF web pages: http://www.metoffice.gov.uk

EUMETSAT ATOVS Retransmission Service Technical Description EUM TD 14, 2004 available from the EUMETSAT EARS web site http://www.eumetsat.int